Upper limits on protolunar disc masses using ALMA observations of directly imaged exoplanets

Sebastián Pérez, Sebastián Marino, Simon Casassus, Clément Baruteau, Alice Zurlo, Christian Flores, Gael Chauvin

Monthly Notices
of the
ROYAL ASTRONOMICAL SOCIETY

MNRAS **488,** 1005–1011 (2019)
Advance Access publication 2019 July 5

doi:10.1093/mnras/stz1775

Upper limits on protolunar disc masses using ALMA observations of directly imaged exoplanets

Sebastián Pérez [1,2]★ Sebastián Marino [3]★ Simon Casassus [1] Clément Baruteau,[4] Alice Zurlo,[5,6] Christian Flores[7] and Gael Chauvin[8,9]

[1] *Universidad de Santiago de Chile, Av. Ecuador 3659, Santiago*
[2] *Departamento de Astronomía, Universidad de Chile, Casilla 36-D, Santiago*
[3] *Max Planck Institute for Astronomy, Königstuhl 17, D-69117 Heidelberg, Germany*
[4] *IRAP, Université de Toulouse, CNRS, UPS, F-31400 Toulouse, France*
[5] *Núcleo de Astronomía, Facultad de Ingeniería y Ciencias, Universidad Diego Portales, Av. Ejercito 441, Santiago, Chile*
[6] *Escuela de Ingeniería Industrial, Facultad de Ingeniería y Ciencias, Universidad Diego Portales, Av. Ejercito 441, Santiago, Chile*
[7] *Institute for Astronomy, University of Hawaii at Manoa, 640 N. Aohoku Place, Hilo, HI 96720, USA*
[8] *Unidad Mixta Internacional Franco-Chilena de Astronomía, CNRS/INSU UMI 3386, Chile*
[9] *Univ. Grenoble Alpes, CNRS, IPAG, F-38000 Grenoble, France*

Accepted 2019 June 24. Received 2019 June 21; in original form 2019 March 4

ABSTRACT

The Solar system gas giants are each surrounded by many moons, with at least 50 prograde satellites thought to have formed from circumplanetary material. Just like the Sun is not the only star surrounded by planets, extrasolar gas giants are likely surrounded by satellite systems. Here, we report on Atacama Large Millimeter/Submillimeter Array (ALMA) observations of four <40 Myr old stars with directly imaged companions: PZ Tel, AB Pic, 51 Eri, and κ And. Continuum emission at 1.3 mm is undetected for any of the systems. Since these are directly imaged companions, there is knowledge of their temperatures, masses, and locations. These allow for upper limits on the amount of circumplanetary dust to be derived from detailed radiative transfer models. These protolunar disc models consider two disc sizes: 0.4 and 0.04 times the exoplanet's Hill radius. The former is representative of hydrodynamic simulations of circumplanetary discs, while the latter a case with significant radial drift of solids. The more compact case is also motivated by the semimajor axis of Callisto, enclosing Jupiter's Galilean satellites. All upper limits fall below the expected amount of dust required to explain regular satellite systems ($\sim 10^{-4}$ times the mass of their central planet). Upper limits are compared with viscous evolution and debris disc models. Our analysis suggests that the non-detections can be interpreted as evidence of dust growth beyond metre sizes to form *moonetesimals* in time-scales $\lesssim$10 Myr. This sample increases by 50 per cent the number of ALMA non-detections of young companions available in the literature.

Key words: planets and satellites: detection – planets and satellites: formation – submillimetre: planetary systems.

1 INTRODUCTION

Regular satellites around giant planets are thought to form in circumplanetary discs (CPDs) of gas and dust as by-products of planet formation (Ruskol 1961; Lunine & Stevenson 1982). In our Solar system alone, a total of at least 50 regular satellites orbit the gas giants, including all major moons. These satellite orbits are close to co-planar with the host planet's equatorial plane, much like a miniature version of a planetary system. This is true even for Uranus that has an obliquity of almost 98 deg. Although the masses and numbers of regular satellite systems vary from planet to planet, all regular satellite systems contain a total mass that is $\sim 10^{-4}$ times the mass of their central planet. For instance, there is 2×10^{-4} M_{Jup} worth of regular satellite mass around Jupiter (Canup & Ward 2006). The same holds for Saturn and Uranus.[1] Is this relation a common trait for gas giant exoplanetary systems? It also holds for close-in

★ E-mail: sebastian.astrophysics@gmail.com (SP);
sebastian.marino.estay@gmail.com (SM)

[1] Neptune's late capture of Triton likely disrupted its circumplanetary rings making it an exception.

rocky planetary systems around late-type stars such as Trappist 1 (e.g. Gillon et al. 2017), and in protoplanetary discs around a variety of stars (e.g. Williams & Cieza 2011).

In analogy with the minimum mass Solar nebula concept (Hayashi 1981), a minimum mass subnebula or *circumjovian* disc can be invoked to study the formation of regular satellites, such as the Galilean moons. In the earlier picture (Lunine & Stevenson 1982; Canup & Ward 2002), all the ingredients for the satellites are present from the initial stage. The gases are eventually dispersed while solids are incorporated into the satellites.

Initially, the material within the CPD builds up progressively, supplied by a near constant inflow of gas and solids from dust traps in the outer circumstellar disc (Canup & Ward 2002; Cilibrasi et al. 2018). Three-dimensional (3D) hydrodynamical simulations agree that CPD radii are truncated between a third or half of the planet's Hill radius (e.g. Ayliffe & Bate 2009). Canup & Ward (2006) found that the overall properties of satellite systems develop naturally when satellites grow embedded in these actively supplied CPDs. This model also reproduces the $\sim 10^{-4}$ mass fraction of total satellite mass, as due to a competition between the supply of solids and satellite loss due to orbital decay in presence of circumplanetary gas. Upon entering the CPD, the mm-sized dust quickly drifts inwards. The dust may eventually stall if gas moves radially outwards in the inner parts of the CPD due to meridional circulation linking the circumplanetary and protoplanetary discs (Morbidelli et al. 2014). If so, the mm-sized dust may then form a dense narrow ring where the streaming instability could set in and form the km-sized bodies that will later form satellites (Drążkowska & Szulágyi 2018).

The gas in circumstellar discs is thought to dissipate after just a few million years (e.g. Williams & Cieza 2011). The details of what happens next are not well constrained due to lack of observational evidence. CPDs may remain gravitationally bound to the planet for a time-scale of a few million years to allow enough time to fully develop Galilean-type satellites (Canup & Ward 2002). Turner, Lee & Sano (2014) reports time-scales for full planet growth of 5–50 Myr, during which the CPD slowly depletes and a last generation of satellites arises from the *protolunar* disc phase, generalizing the term 'circumjovian' to a broader sense. Crida & Charnoz (2012) suggests that moons can still form in massive primordial rings when they spread beyond the Roche radius. Kenworthy & Mamajek (2015) reported a system with unusual transits, which they interpret as circumplanetary rings filling most of the Hill radius.

In this work, we report on Atacama Large Millimeter/Submillimeter Array (ALMA) observations (Section 2) of four directly imaged exoplanets[2] with separations <300 au: PZ Tel b, AB Pic b, 51 Eri b, and κ And b. The ages of these systems are between 21 Myr and 47 Myr, i.e. not much older than the CPD depletion time-scale (∼10 Myr, Canup & Ward 2002) after the dissipation of the circumstellar gas. These exoplanets are undetected in our 1.3 mm observations, but the rms levels provide upper limits to the mass reservoir available for satellite formation (Section 3). These upper limits are put into context with previous non-detections from the literature (Section 4).

[2]Although some bodies considered in this work are in the brown dwarf mass regime, we sometimes refer to them as 'exoplanets' as this distinction does not impact our analysis.

2 DATA DESCRIPTION

We used the ALMA to observe four directly imaged exoplanets. We obtained observations at 1.3 mm wavelength using the 12 m array with baselines ranging from 19 m to up to 3.0 km, resulting in an angular resolution of ∼0.15 arcsec (using natural weights), sensitive to spatial scales of up ∼2.0 arcsec. These observations were performed during Cycles 3 and 4 (project IDs `2015.1.01210.S` and `2016.1.00358.S`). The cycling time for phase calibration was set to 2 min. Time on science source varies for each target depending on the exoplanet system properties. On average, each observing block was integrated for ∼38 min in total (including calibrations). The ALMA correlator was configured in Frequency Division Mode. Three spectral windows with 2.0 GHz bandwidth were set up for detecting the dust continuum, centred at 232.469, 217.871, and 215.371 GHz, respectively. A fourth spectral window centred at 230.507 is aimed at probing for ^{12}CO gas emission (1.875 GHz in bandwidth with 960 channels). Searching for low-level gas in these systems is beyond the scope of this paper, and will likely require sophisticated analysis to produce a detection (e.g. by stacking after correcting by Doppler shifts; Marino et al. 2016). Proper motions were accounted for when more than one observing blocks were used to produce a concatenated Measurement Set.

All data were calibrated by the ALMA staff using the ALMA Pipeline in the CASA package (McMullin et al. 2007), including offline Water Vapour Radiometer calibration, system temperature correction, as well as bandpass, phase, and amplitude calibrations. Image reconstruction was performed using the CLEAN algorithm (CASA v.5.2, task `tclean`) with 'natural' weights. All spectral windows were combined in the imaging. No sources were detected in our observations. The rms value for each data set was calculated from the CLEAN ed images and are reported in Table 1.

3 CPD MODELS AND DUST MASS UPPER LIMITS

For all selected candidates, we modelled the protolunar discs as dusty discs with a surface density profile equivalent to a self-similar solution for a viscous accretion disc (Lynden-Bell & Pringle 1974). We used a power-law slope of −1 and an exponential cut-off radius r_c of 0.4 times the planet's Hill radius (R_H) as our fiducial model (Ayliffe & Bate 2009). An alternative model with $r_c = 0.04R_H$ (about the size of the Galilean moon system) is also considered to show how sensitive the derived mass is to the disc radius. The minimum radius of the grid is $r_c/10$. If dust temperatures rise above the sublimation temperature, the disc inner radius is increased. A constant disc vertical aspect ratio of 0.1 is assumed.[3] A finite relative inclination of 2 deg between the orbit of each planet and its CPD is used, motivated by regular satellites in the Solar system that have orbital inclinations ranging from less than a degree up to 2 deg.

The dust is assumed to follow a size distribution from 1 μm to 1 cm (following a power-law exponent of −3.5) and it is composed of astrosilicates, amorphous carbon, and water ice. This yields an absorption opacity of 2.3 cm^2 g^{-1} at 1.3 mm. We input our model into the RADMC3D radiative transfer (RT) code to calculate the total flux expected at 1.3 mm (Dullemond et al. 2012). Both dust thermal emission and scattering (anisotropic) are considered

[3]Dust vertical scale-heights are dependent on Stokes number and α viscosity. We tested how our approximation compares for the case of PZ Tel and found that a more realistic scale-height only affects the emitted fluxes by $\lesssim$10 per cent when compared to a constant aspect ratio for all species.

Table 1. Millimetre and sub-millimetre continuum observations of protolunar discs. Note that the stellar age and some of the exoplanet parameters (e.g. mass) are uncertain, hence the values used here serve simply as order of magnitude estimates.

Exoplanet system	Age (Myr)	D^a (pc)	Stellar parameters $M_\star$($M_\odot$)	$R_\star$ ($R_\odot$)	$T_\star$ (K)	Exoplanet or companion parameters a (au)	M_p (M_J)	R_p ($R_\odot$)	T_p (K)^b	3σ limit (μJy)	M_{max}/M_p $r_c = 0.4R_{Hill}$	$r_c = 0.04R_{Hill}$	Refs
PZ Tel b	21	47	1.0	1.32	5250	25	38	0.25	2700	84	2.5×10^{-7}	2.0×10^{-7}	1,2
51 Eri b	21	30	1.75	1.5	7250	13	2	0.08	750	81	2.2×10^{-6}	-	3
AB Pic b	30	50	0.8	1.0	5000	260	13	0.15	1600	78	5.0×10^{-6}	2.4×10^{-6}	4,5
κ And b	47	50	2.5	2.3	11500	53	22	0.25	2040	180	9.0×10^{-7}	1.4×10^{-6}	6,7,8
Previous 1.3 mm observations from Booth et al. (2016)													
HR 8799 b	42	41	1.5	1.5	7250	70	5.8	0.12	870	48	1.1×10^{-6}	1.5×10^{-6}	9, 10, 24
HR 8799{c,d,e}	42	41	1.5	1.5	7250	{43, 26, 15}	7.2	0.1	1100	48	{0.9,1.0,1.0} $\times 10^{-6}$	{1.2,1.4,1.6} $\times 10^{-6}$	9, 10, 24
Previous 1.3 mm observations from Wu et al. (2017b)													
DH Tau b	2	135	0.5	0.5	3600	317	15	0.25	2400	129	5.0×10^{-5}	1.8×10^{-6}	11,12,13
CT Cha b	2	192	0.6	0.65	4000	512	20	0.22	2600	150	9.0×10^{-6}	4.3×10^{-5}	11,14
GSC6214-210 b	10	109	0.9	1.0	4400	236	15	0.19	2200	90	6.0×10^{-6}	2.5×10^{-6}	11,15
1RXS1609 b	10	140	0.85	1.3	4060	308	13	0.17	2000	90	2.0×10^{-5}	7.0×10^{-6}	11,16
GQ Lup b	3	152	1.0	1.7	4300	109	25	0.33	2400	120	4.5×10^{-6}	3.7×10^{-6}	17
Previous 0.89 mm observations from Ricci et al. (2017)													
2M1207 b	8	52	0.023	0.36	2500	41	4	0.12	1100	78	1.5×10^{-6}	1.8×10^{-6}	18,19,20,21
Previous 1.3 mm observations from Matrà et al. (2019)													
β Pic b	21	20	1.75	1.5	8250	9	11	0.15	1600	36	4.0×10^{-8}	4.0×10^{-7}	22,23
Previous 1.3 mm observations from Su et al. (2017)													
HD 95086 b	17	84	1.6	1.6	7550	62	4.4	0.12	1050	30	3.5×10^{-6}	8.0×10^{-6}	25,26

References: 1. Maire et al. (2016), 2. Pecaut, Mamajek & Bubar (2012), 3. Macintosh et al. (2015), 4. Bonnefoy et al. (2010), 5. Chauvin et al. (2005b), 6. Bonnefoy et al. (2014), 7. Hinkley et al. (2013), 8. Jones et al. (2016), 9. Marois et al. (2008), 10. Booth et al. (2016), 11. Wu et al. (2017b), 12. Wolff et al. (2017), 13. Zhou et al. (2014), 14. Wu et al. (2015a), 15. Bowler et al. (2015), 16. Wu et al. (2015b), 17. Wu et al. (2017a), 18. Chauvin et al. (2004), 19. Chauvin et al. (2005a), 20. Ricci et al. (2017), 21. Song et al. (2006), 22. Lagrange et al. (2009), 23. Lagrange et al. (2018), 24. Bonnefoy et al. (2016), 25. Su et al. (2017), 26. Zapata, Ho & Rodríguez (2018).

[a] *GAIA* Data Release 2.

[b] Planet temperatures are constrained from observations assuming a hot start model.

in the RT calculation. The star and planet luminosities are included as energy sources that set the dust temperature. Finally, in order to derive an upper limit for the total dust mass, we varied the disc mass until the 3σ flux upper limit is matched for each disc. When computing images and observed fluxes we assumed disc inclinations of 30 deg from face on for all systems, except for β Pic b, which we assumed to be inclined by 85 deg and co-planar with the circumstellar debris disc (Lagrange et al. 2018; Matrà et al. 2019). We note that this inclination only makes a difference if the discs are massive enough to become optically thick in the radial direction at 1.3 mm. The rms value for β Pic b is calculated as the thermal noise in a region devoid of circumstellar emission. We interpret this as an upper limit since upon subtraction of a parametric model for the disc, there is no point-like emission above 3σ (Matrà et al. 2019).

In Table 1 and Fig. 1, we present the dust mass upper limits derived from the RT calculations. The limits are lower for the closest systems as expected, and the ones with shorter planet semimajor axis since this makes discs warmer and brighter for the same dust mass. The lowest of these limits is for β Pic b because it has the deepest ALMA observations, it is the closest system from our sample, and has the highest temperature field since it is the closest to its central star. For all systems, the dust mass upper limits lie below the expected total mass in solids if exoplanets have the same mass ratio between the total mass in satellites and planet ($2 \times 10^{-4} M_p$, where M_p is the mass of the exoplanet, see grey band in Fig. 1). This means that there is not enough mass in dust to form Jovian-like systems, or that satellites must have already formed or grown to planetesimal sizes that are transparent at $\sim$1 mm.

In Fig. 1, we overlay (dashed lines) the dust masses at which discs become optically thick (assuming constant surface densities). We find that for cut-off radii of 0.4 R_H, all discs are optically thin at 1.3 mm (left-hand panel). However, if discs are an order of magnitude smaller in radius, the protolunar discs around 51 Eri b and β Pic b become optically thick at 1.3 mm. In fact, the upper limit for 51 Eri b is higher than the maximum possible flux of a CPD in this system (in the compact case the disc is highly optically thick). Therefore, our flux upper limit for 51 Eri b does not place a constraint on the disc mass in the small disc scenario.

The limits derived here can be compared to results by Ricci et al. (2017) that assumed optically thin emission and a single dust temperature scaling with stellar luminosity. We find limits for DH Tau b, GSC 6214-210 B, and GQ Lup b that are consistent within a factor of a few when assuming a large cut-off radius, but much lower for DH Tau b if its disc is compact and thus warmer as the heat from the planet has a larger impact. For 2M1207 b, we find a mass that is a factor of 2 lower, which can be explained by the higher temperature in our models compared to the one used by Ricci et al. (2017). In our RT model, both the stellar and planet luminosities are included as heating sources, thus the large dust grains have temperatures of $\sim$30 K (between 1 and 10 au), versus the 8 K assumed in the previous study.

4 DISCUSSION

The upper limits derived in the previous section are put into context of two simple evolution models: (1) viscous evolution of a gas disc and (2) collisional evolution of a planetesimal disc replenishing a population of mm-sized dust. These provide order of magnitude estimates for the expected dust mass in CPDs as a function of age, planet and stellar mass, and semimajor axis.

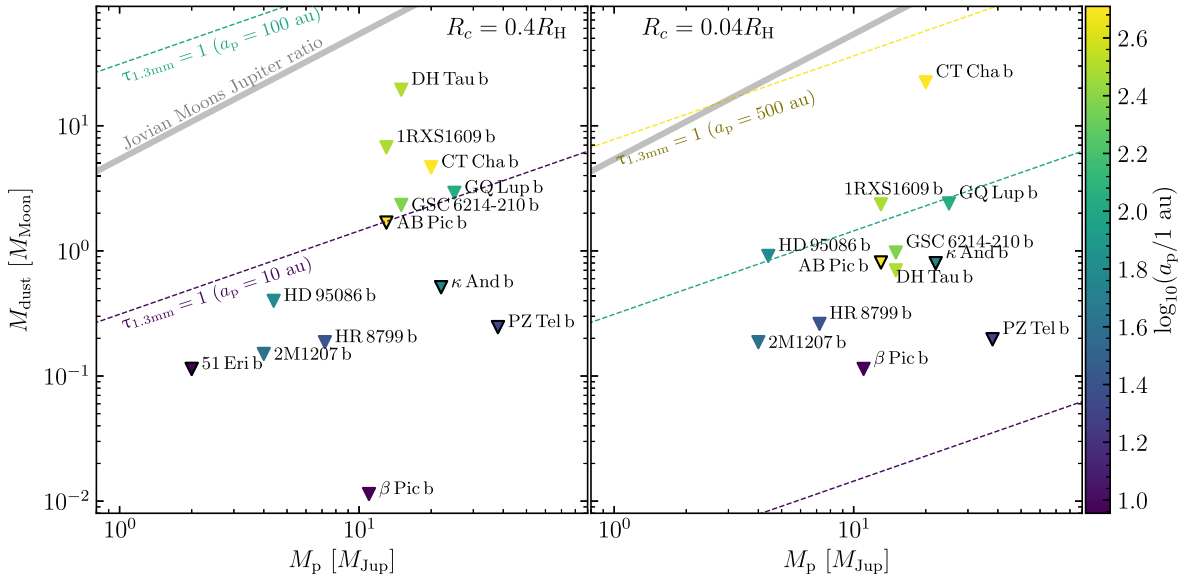

Figure 1. Dust mass upper limits of directly imaged exoplanets and sub-stellar companions observed at 0.89 and 1.3 mm, as a function of planet mass. The colour of each marker represents the semi-major axis of each planet, which is estimated based on the deprojected separation. The four new ALMA observations are highlighted with black edges. Calculations are shown for two protolunar disc sizes: cut-off radii of 0.4 (left) and 0.04 (right) times the planet's Hill radius. The dust masses at which the discs become optically thick in the vertical direction at 1.3 mm are represented by dashed lines for different planet semimajor axes. 51 Eri b does not feature in the compact disc case, as it is highly optically thick and unconstraining.

4.1 Viscous evolution

For the viscous evolution scenario, we assume an α disc model where each planet is initially surrounded by an accretion disc rich in gas and dust (gas-to-dust ratio of 100), with an initial solid mass of $10^{-4}M_p$, where dust particles are smaller than the molecular mean-free path, i.e. the Epstein regime, where dust and gas are well coupled (this might not be valid for low gas densities as large dust grains experience radial drift due to aerodynamics drag). The dimensionless stopping time or Stokes number (St) is proportional to the dust size over the gas surface density, for a given grain internal density. For a vertically isothermal disc, St can be written as

$$\mathrm{St} \approx 0.1 \left(\frac{a}{1_{\mathrm{mm}}}\right) \left(\frac{M_{\mathrm{dust}}/M_p}{10^{-4}}\right)^{-1} \left(\frac{a_p}{50\,\mathrm{au}}\right)^2 \left(\frac{M_p/M_\star}{10^{-2}}\right)^{2/3} \left(\frac{r_c}{0.4R_H}\right)^2, \quad (1)$$

where we assume a grain internal density of 1 g cm^3. Millimetre-sized dust would only be well coupled to the gas (St $<<1$) if disc masses are $\gtrsim 10^{-2}M_p$ or discs have $r_c \lesssim 0.4R_H$. Otherwise, large dust grains containing the bulk of the solid mass will quickly migrate inwards. Therefore, the model presented here provides only an upper limit for the expected dust masses if the only loss process is the viscous accretion.

For the viscous evolution, we assumed an α-disc model (Lynden-Bell & Pringle 1974) where viscosity scales linearly with radius, such that

$$\Sigma(r, \widetilde{T}) = \Sigma_0 \left(\frac{r}{r_0}\right)^{-1} \exp\left[-\left(\frac{r}{r_0 \widetilde{T}}\right)\right] \widetilde{T}^{-3/2}, \quad (2)$$

where $\widetilde{T} = (t/t_{\nu,0} + 1)$ and $t_{\nu,0} = r_0^2/(3\nu)$ is the viscous time-scale evaluated at r_0 (the initial cut-off radius). The CPD viscous evolution is calculated after the protoplanetary disc starts dissipating (we assume a dissipation time-scale of 1 Myr). For the disc viscosity, we used equation 18 from Zhu, Andrews & Isella (2018), assuming a disc temperature of 40 K (this value is consistent with the temperature at 1 au from the planet in our models). Then, the disc surface density and mass should decrease with time as $t^{-3/2}$ and $t^{-1/2}$, with the gas cut-off radius increasing linearly with time as is the case for a freely expanding disc. However, this spreading does not happen perpetually since the CPD must be truncated. Here, we choose a truncation radius $r_t = 0.4R_H$, motivated by 3D hydrodynamic simulations of CPDs (e.g. Ayliffe & Bate 2009), and assume that at $t = 1$ Myr the gas cut-off radius is already equal to r_t. Therefore, for the evolution after 1 Myr instead we used equation 5 in Rosotti & Clarke (2018) that describes the exponential decay of a viscous disc around a companion (in the context of binary interactions). The characteristic time-scale of the evolution is $t_t = 16r_t^2/(3\pi^2\nu_c)$, where ν_c is the viscosity evaluated at r_t. In this manner then, the gas and dust mass evolve as

$$M(t) = M_0 \exp\left(-\frac{t - t_c}{t_t}\right). \quad (3)$$

In Fig. 2, we compare the dust mass upper limits with the expected viscous evolution of the dust mass as a function of system's age. Note that the age of these systems is uncertain and could vary by ~50 per cent. The dashed and dotted lines represent models with $\alpha = 10^{-4}$ and 10^{-3}, respectively. The green and purple lines correspond to models for planet masses of 20 and 2M$_{\mathrm{Jup}}$, respectively. Note that even if we had considered a smaller initial cut-off radius, the viscous evolution would be very similar since an initially small disc will spread quickly until reaching the truncation radius, after which it will decay exponentially. We find that, for the high α viscosity case, all our upper limits are above the model predictions by orders of magnitude for both disc sizes $0.4R_H$ and $0.04R_H$ (left-hand and right-hand panels, respectively), except for CT Cha when $r_0 = 0.4R_H$, DH Tau when $r_0 = 0.04R_H$ and GQ Lup in both cases. This is because these systems are the youngest, thus they are more likely to have a large dust mass in this scenario. In the low α case, the disc evolution is slower and our upper limits for planets with masses above ~10 M$_{\mathrm{Jup}}$ lie below the model curves. On

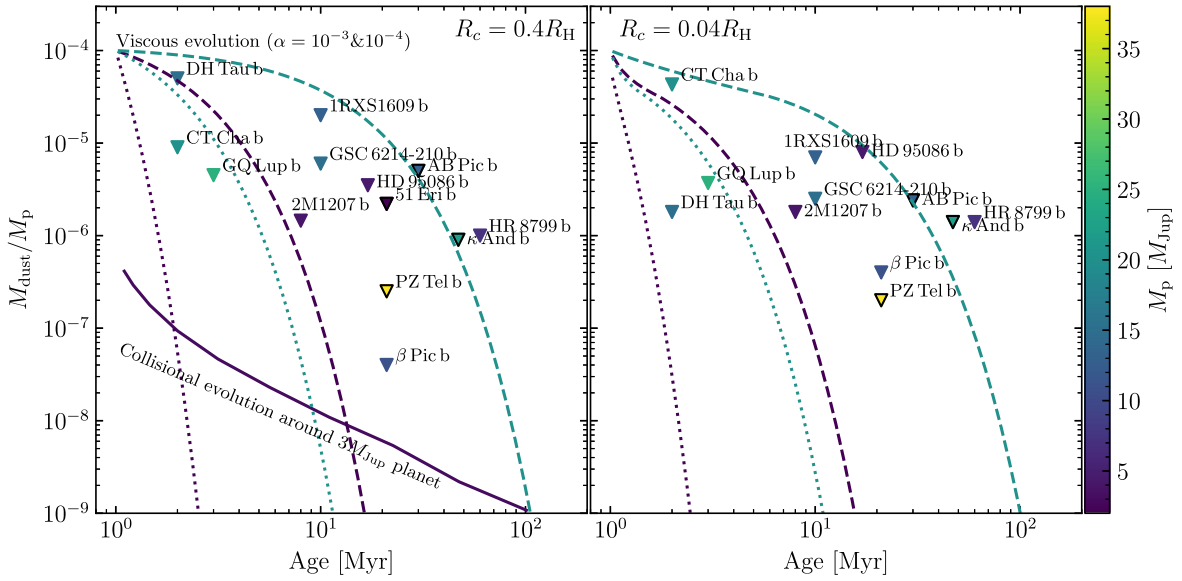

Figure 2. Upper limits on the ratio of dust mass to planet mass for directly imaged exoplanets observed at 0.89 and 1.3 mm as a function of stellar age, based on disc models with two cut-off radii: 0.4 (left) and 0.04 (right) times the planet Hill radius. The dashed and dotted lines represent viscous evolution models with $\alpha = 10^{-4}$ and 10^{-3}, respectively, and surrounding planets with masses of 2 (purple) and 20M_{Jup} (green). The continuous purple line represents the dust levels expected if mm-sized dust was created in a collisional cascade in a debris disc around a 3M_{Jup} planet.

the other hand, the viscous time-scale around lower mass planets is shorter and thus our model predicts masses that are orders of magnitude lower than the upper limits. Based on our upper limits, we conclude that either CPDs around the more massive of our companions evolve faster than models with $\alpha \gtrsim 10^{-4}$, or mm-size grains are lost through radial drift or grow into larger objects with very low opacities at millimetre wavelengths.

4.2 Collisional evolution

An alternative scenario for the presence of dust in CPDs is to consider secondary origin dust created from collisions of planetesimals, i.e. like a debris disc (for a detailed discussion see Kennedy et al. 2011). Such a disc will collisionally evolve and its mass will decrease with time as planetesimals are ground down to the size of small grains blown out by radiation from the planet or perturbed to $e > 1$ by the stellar radiation (Burns, Lamy & Soter 1979). In order to compute predictions for the evolution of the disc mass in dust smaller than 1 cm, we used the model presented in Marino et al. (2017). This model requires several input parameters, e.g. the initial mass in solids, planetesimal strength, level of stirring. We used standard values used to model circumstellar debris discs for the planetesimal strength and density, and we set the rest of the parameters to extremes to obtain the most favourable condition to detect such disc, i.e. slow evolution and high initial mass. We assumed a planetesimal mean eccentricity and inclination of 0.01 and 0.005; disc radius of 0.4 R_H with a fractional width of 0.5 to maximize the volume; planet semimajor axis 30 au; and a planet mass of 3 M_{Jup} (at the lower end of the distribution) such that the orbital frequency and collisional rates are low. Finally, we considered a large maximum planetesimal size of 100 km to slow down the collisional evolution, and an extreme initial solid mass of $10^{-3}M_p$ (or $\sim 10^{-7}M_p$ in mm-sized dust, assuming a size distribution with an exponent of -3.5) to estimate the maximum mass of collisionally produced dust that could be present.

In the left-hand panel of Fig. 2, the evolution of the dust mass in a massive planetesimal disc is shown assuming planetesimals are stirred at 1 Myr (purple line). The dust mass predicted by this model is orders of magnitude lower than our upper limits. Higher planet masses, smaller discs in units of R_H, higher planetesimal eccentricities, or inclinations would make this evolution even faster. Therefore, we do not expect to observe debris disc like dust around directly imaged planets, unless the solid mass is being replenished (e.g. from a circumstellar planetesimal belt) or large amounts of dust were recently produced is a stochastic collision between moon embryos.

4.3 Maximum-grain sizes

Given the derived upper limits on the solid mass in the form of dust smaller than 1 cm presented in Section 3, and by assuming a size distribution and a total mass of solids, we can derive a lower limit on the maximum size of particles in these circumplanetary or protolunar discs. In particular, here we assume a power-law size distribution with an exponent of -3.5 and a total solid mass equivalent to $10^{-4}M_p$. The solid size lower limits are then simply

$$D_{max} = 2\ \mathrm{cm} \left(\frac{10^{-4} M_p}{M_{dust}} \right)^2, \quad (4)$$

where D_{max} is the diameter of the largest object in the disc. In Fig. 3, we show lower limits on D_{max} based on the derived upper limits on M_{dust}.[4] The non-detections translate to a value of D_{max} >1 m for most sources. Therefore, we conclude that dust growth beyond metre sizes must happen in time-scale $\lesssim 10$ Myr. After this time-scale, the solid material is likely in *moonetesimal* form.

The working hypothesis that motivated the observations and the analysis presented here assumed that satellite formation is

[4]We consider the largest upper limit on M_{dust} between both dust disc sizes (0.4 R_H and 0.04 R_H).

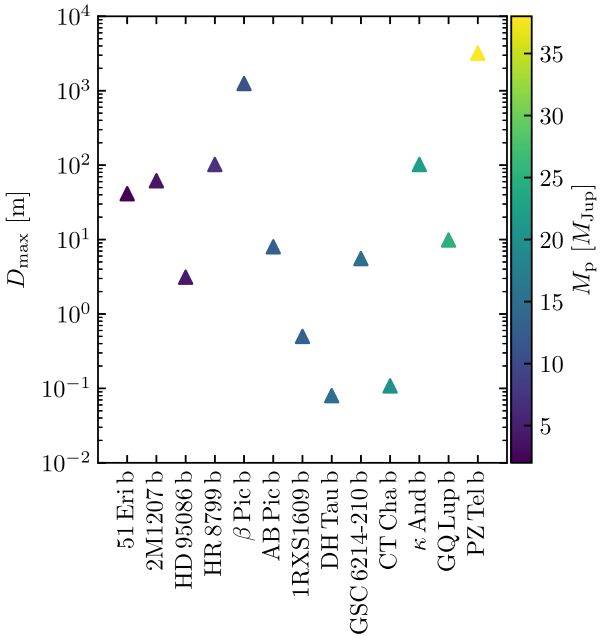

Figure 3. Lower limits on the maximum diameter of solids around each directly imaged companion based on our dust upper limits and assuming a solid size distribution with an exponent of −3.5 and a total solid mass of 10^{-4} $M_{\rm p}$. Sources are sorted by planet mass, with the less massive companions on the left, and the most massive on the right.

a common occurrence. Although common in the Solar system, the lack of detection of circumplanetary material around young exoplanets could also imply that these planets do not form satellites.

5 CONCLUDING REMARKS

We presented ALMA observations of four young systems host to directly imaged exoplanets and sub-stellar companions. Upper limits to the mass in $\lesssim$mm dust around these planets have been drawn from the rms levels using detailed RT modelling. All upper limits fall below the expected amount of dust and debris required to explain regular satellite systems ($\sim 10^{-4}\,M_{\rm p}$). We interpret this as likely evidence for rapid growth of dust into $\gtrsim$1 m planetesimals (or rather *moonetesimals*), which lowers the protolunar disc opacity at mm wavelengths.

The detection of protolunar discs in dust emission at radio wavelengths needs deep observations of the youngest exoplanets (e.g. DH Tau, CT Cha, and GQ Lup) that reach several times higher sensitivities than current reported observations.

Ongoing observations of dust around accreting planets still embedded in their protoplanetary discs (e.g. HD 100546, Pérez, et al. 2019, and PDS 70, Christiaens, et al. 2019; Isella et al. 2019) could provide further constraints on the time-scales for satellites formation.

ACKNOWLEDGEMENTS

We thank the anonymous referee for their constructive comments. We acknowledge support from the Millennium Science Initiative (Chile) through grant RC130007 and CONICYT-FONDECYT grant numbers 1171624, 1171246 and 1191934. SP acknowledges support from the Joint Committee of ESO and the Government of Chile. This work used the Brelka cluster, financed by Fondequip project EQM140101, hosted at DAS/U. de Chile. AZ acknowledges support from the CONICYT-PAI, Convocatoria nacional subvención a la instalación en la academia, convocatoria 2017, Folio PAI77170087.

REFERENCES

Ayliffe B. A., Bate M. R., 2009, MNRAS, 397, 657
Bonnefoy M., Chauvin G., Rojo P., Allard F., Lagrange A.-M., Homeier D., Dumas C., Beuzit J.-L., 2010, A&A, 512, A52
Bonnefoy M. et al., 2014, A&A, 562, A111
Bonnefoy M. et al., 2016, A&A, 587, A58
Booth M. et al., 2016, MNRAS, 460, L10
Bowler B. P., Andrews S. M., Kraus A. L., Ireland M. J., Herczeg G., Ricci L., Carpenter J., Brown M. E., 2015, ApJ, 805, L17
Burns J. A., Lamy P. L., Soter S., 1979, Icarus, 40, 1
Canup R. M., Ward W. R., 2002, AJ, 124, 3404
Canup R. M., Ward W. R., 2006, Nature, 441, 834
Chauvin G., Lagrange A.-M., Dumas C., Zuckerman B., Mouillet D., Song I., Beuzit J.-L., Lowrance P., 2004, A&A, 425, L29
Chauvin G., Lagrange A.-M., Dumas C., Zuckerman B., Mouillet D., Song I., Beuzit J.-L., Lowrance P., 2005a, A&A, 438, L25
Chauvin G. et al., 2005b, A&A, 438, L29
Christiaens V., Cantalloube F., Casassus S., Price D. J., Absil O., Pinte C., Girard J., Montesinos M., 2019, ApJ, 877, L33
Cilibrasi M., Szulágyi J., Mayer L., Drążkowska J., Miguel Y., Inderbitzi P., 2018, MNRAS, 480, 4355
Crida A., Charnoz S., 2012, Science, 338, 1196
Drążkowska J., Szulágyi J., 2018, ApJ, 866, 142
Dullemond C. P., Juhasz A., Pohl A., Sereshti F., Shetty R., Peters T., Commercon B., Flock M., 2012, Astrophysics Source Code Library, record ascl:1202.015
Gillon M. et al., 2017, Nature, 542, 456
Hayashi C., 1981, Prog. Theor. Phys. Suppl., 70, 35
Hinkley S. et al., 2013, ApJ, 779, 153
Isella A., Benisty M., Teague R., Bae J., Keppler M., Facchini S., Pérez L. M., 2019, preprint (arXiv:1906.06308)
Jones J., White R. J., Quinn S., Ireland M., Boyajian T., Schaefer G., Baines E. K., 2016, ApJ, 822, L3
Kennedy G. M., Wyatt M. C., Su K. Y. L., Stansberry J. A., 2011, MNRAS, 417, 2281
Kenworthy M. A., Mamajek E. E., 2015, ApJ, 800, 126
Lagrange A.-M. et al., 2009, A&A, 493, L21
Lagrange A.-M. et al., 2018, A&A, 621, L8
Lunine J. I., Stevenson D. J., 1982, Icarus, 52, 14
Lynden-Bell D., Pringle J. E., 1974, MNRAS, 168, 603
Macintosh B. et al., 2015, Science, 350, 64
Maire A.-L. et al., 2016, A&A, 587, A56
Marino S. et al., 2016, MNRAS, 460, 2933
Marino S., Wyatt M. C., Kennedy G. M., Holland W., Matrà L., Shannon A., Ivison R. J., 2017, MNRAS, 469, 3518
Marois C., Macintosh B., Barman T., Zuckerman B., Song I., Patience J., Lafrenière D., Doyon R., 2008, Science, 322, 1348
Matrà L., Wyatt M. C., Wilner D. J., Dent W. R. F., Marino S., Kennedy G. M., Milli J., 2019, AJ, 157, 135
McMullin J. P., Waters B., Schiebel D., Young W., Golap K., 2007, ASPC, 376, 127
Morbidelli A., Szulágyi J., Crida A., Lega E., Bitsch B., Tanigawa T., Kanagawa K., 2014, Icarus, 232, 266.
Pecaut M. J., Mamajek E. E., Bubar E. J., 2012, ApJ, 746, 154
Pérez S. et al., 2019, preprint (arXiv:1906.06305)
Ricci L., Rome H., Pinilla P., Facchini S., Birnstiel T., Testi L., 2017, ApJ, 846, 19
Ricci L. et al., 2017, AJ, 154, 24
Rosotti G. P., Clarke C. J., 2018, MNRAS, 473, 5630
Ruskol E. L., 1961, SvA, 4, 657

Song I., Schneider G., Zuckerman B., Farihi J., Becklin E. E., Bessell M. S., Lowrance P., Macintosh B. A., 2006, ApJ, 652, 724
Su K. Y. L. et al., 2017, AJ, 154, 225
Turner N. J., Lee M. H., Sano T., 2014, ApJ, 783, 14
Williams J. P., Cieza L. A., 2011, ARA&A, 49, 67
Wolff S. G. et al., 2017, AJ, 154, 26
Wu Y.-L. et al., 2015a, ApJ, 801, 4
Wu Y.-L. et al., 2015b, ApJ, 807, L13
Wu Y.-L. et al., 2017a, ApJ, 836, 223
Wu Y.-L., Close L. M., Eisner J. A., Sheehan P. D., 2017b, AJ, 154, 234
Zapata L. A., Ho P. T. P., Rodríguez L. F., 2018, MNRAS, 476, 5382
Zhou Y., Herczeg G. J., Kraus A. L., Metchev S., Cruz K. L., 2014, ApJ, 783, L17
Zhu Z., Andrews S. M., Isella A., 2018, MNRAS, 479, 1850

This paper has been typeset from a TEX/LATEX file prepared by the author.